Applied Geochemistry 175 (2024) 106145

Contents lists available at ScienceDirect

Applied Geochemistry

journal homepage: www.elsevier.com/locate/apgeochem

Gluconate and formate uptake by hydrated cement phases

Rosa Ester Guidone [a,b,*], Xavier Gaona [b], Marcus Altmaier [b], Barbara Lothenbach [a]

[a] Empa (Swiss Federal Laboratories for Materials Science and Technology), Überlandstrasse 129, 8600, Dübendorf, Switzerland
[b] Karlsruhe Institute of Technology (KIT), Institute for Nuclear Waste Disposal (INE), Hermann-von-Helmholtz-Platz 1, 76344 Eggenstein-Leopoldshafen, Germany

ARTICLE INFO

Editorial Handling by: Erich Wieland

Keywords:
Gluconate
Formate
C–S–H phases
AFm phases
Ettringite
Portland cement
Uptake

ABSTRACT

The uptake of formate and gluconate by C–S–H, AFm phases, ettringite and hydrated Portland cement (PC) was studied at pH 13 by batch sorption experiments. The formation of gluconate and formate-AFm phases was observed in pure systems, but not in hydrated cement. Gluconate sorbs more strongly on AFm phases and ettringite than formate. Higher calcium concentrations increase the gluconate sorption on C–S–H and hydrated Portland cements due the formation of Ca-gluconate surface complexes on C–S–H. Measured R_d values for gluconate sorption on C–S–H increase from 2.0 $dm^3 \cdot kg^{-1}$ for C–S–H with Ca/Si = 0.8 to 34 $dm^3 \cdot kg^{-1}$ for Ca/Si = 1.4 at pH 13. They are a factor 5 to 10 higher at lower pH values, and higher Ca-concentrations. Calcium concentration does not significantly affect the uptake of formate by C–S–H. Formate sorbs on hydrated PC with R_d values in the range of 3–33 $dm^3 \cdot kg^{-1}$.

1. Introduction

Organic additives are widely used to control and adjust the workability, durability and strength of cementitious materials. The added amount (Ma et al., 2015; Perez, 2007) and the order of addition of cement additives may alter the properties of cement (von Daake and Stephan, 2017).

Sodium gluconate ($Na(C_6H_{12}O_7)$, Na-GLU) is commonly used as a retarder (Nafee et al., 2023; Perez, 2007; Singh, 1976; Zhang et al., 2017) and can, when combined with a superplasticizer, alter the fluidity of the cement paste (Li et al., 2012; Zou et al., 2017) and the setting time (Li et al., 2018). Singh (1976) suggested that gluconate poisons the hydrates nuclei on the surface of C_3S grains, but as soon as gluconate is completely adsorbed and the fresh nuclei are formed, the hydration process accelerates again. (Perez, 2007) showed that gluconate sorbs specifically on alite (C_3S) and gluconate uptake depends on the dosage. At low gluconate dosages (0.09 wt%), gluconate sorbs weakly on aluminate-sulfate phases (responsible for the formation of AFm phases and ettringite) and has a small effect on the congruent dissolution of alite. At higher dosage (> 0.13 wt%), gluconate can also adsorb on alite surface, thus inhibiting the initial C–S–H formation and increasing the induction period. High gluconate dosage inhibits also slightly the hydration of the aluminates. (Ma et al., 2015) showed the delayed formation of ettringite and inhibition of gypsum dissolution for a gluconate dosage higher than 0.05% dry cement.

Formate ($HCOO^-$, FOR) is a known cement accelerator and is also used as antifreezing additive for concretes (Hartmann et al., 2014; Vdovin and Stroganov, 2020). Hewlet (1998) compared the calcium salts of chloride, nitrite and formate, and related their accelerating efficiency to the mobility of the anions within the silicate particles, concluding that the anion size is a major factor. Due to its larger size (0.45 nm), formate is less suitable as accelerator than anions with smaller size such as nitrite (0.34 nm) or chloride (0.27 nm) (Hewlet, 1998). It was observed that the presence of formate accelerates the precipitation of $Ca(OH)_2$ as well as the reaction of C_3S and C_2S (Heikal, 2004). Calcium formate $Ca(HCOO)_2$ has a relatively low solubility in water (approx. 16g/100 g H_2O at room temperature), such that it must be added to concrete or cement mixture in solid form. Sodium formate, which has also accelerating properties (Gebler, 1983), is approximately 3 times more soluble in water, but it leads to the increase of alkali content to the mixture, which can contribute to the formation of alkali silica products responsible for expansion and cracking of concrete (Lindgård et al., 2012).

In the context of cement-based repositories for the disposal of low and intermediate level radioactive waste (L/ILW), the presence of low molecular weight organics such as gluconate, α-isosaccharinate or formate needs to be taken into account in the evaluation of the long-term safety of the repository. The presence of low molecular weight organics may alter the solubility and sorption properties of radionuclides in the cement matrix, possibly influencing the migration of these

* Corresponding author. Empa (Swiss Federal Laboratories for Materials Science and Technology), Überlandstrasse 129, 8600, Dübendorf, Switzerland.
E-mail address: rosa.guidone@kit.edu (R.E. Guidone).

https://doi.org/10.1016/j.apgeochem.2024.106145
Received 15 February 2024; Received in revised form 24 July 2024; Accepted 16 August 2024
Available online 20 August 2024

radionuclides. Low molecular weight organics are found in the repository either as a component in the cement formulations (e.g., cement additives), as part of the emplaced waste (e.g., decontaminating agents such as EDTA, NTA or citrate), as degradation products of complex organic materials (e.g., cellulosic materials), or present as ^{14}C containing organic compounds in core structural material and reactor coolant waste streams (Ochs et al., 2016; Wieland and Hummel, 2015).

Only a few studies have previously investigated the uptake of formate by hardened cement paste (HCP) (Kaneko et al., 2002; Wieland et al., 2016). Wieland et al. (2016) investigated the sorption of several ^{14}C labelled small organic molecules (i.e. formic acid, acetic acid, acetaldehyde, formaldehyde, ethanol, methanol) on HCP (S/L = 333 g·dm^{-3}) and AFm phases, such as monosulphate (Ms), hemicarbonate (Hc), monocarbonate (Mc) and ettringite. The authors observed that the strength of the uptake for the investigated organics followed the sequence alcohol < aldehyde < carboxylate and that the uptake of formate was stronger than of acetate. At a contact time of 90 days, formate sorbed on hydrated cement phases in the following order: C–S–H > Hc > Ms ~ AFt > Mc. The partition coefficient (R_d) of the investigated organic molecules on HCP and individual cement phases ranged from 0.01 to 1 dm^3·kg^{-1}. This is also in agreement with a recent investigation on Portland cement (PC), where only a weak to moderate uptake of formate by hydrated cement was observed (Nedyalkova et al., 2021).

The uptake of GLU and α-ISA (α-isosaccharinate, a main degradation product of cellulose and chemical analogue of GLU) by cement and C–S–H phases has been extensively investigated in the last 30 years. (Glaus et al., 2006) investigated the uptake of GLU and α-ISA by HCP using an artificial cement pore water corresponding to the first degradation stage of cement (ACW, pH = 13.4, Na = 114 mM, K = 180 mM, Ca = 2 mM). Sorption data were interpreted using a two-site Langmuir isotherm, which postulates the presence of two (strong and weak) sorption sites. The uptake of gluconate was slightly stronger than the uptake of α-ISA and distribution ratios of $R_d \approx 3–4{\cdot}10^3$ dm^3·kg^{-1}for $[GLU]_{tot} = 10^{-7}–10^{-4}$ M were observed. Desorption of sorbed gluconate species was found to be strongly kinetically inhibited due to the strong interaction with active sites of cement (and C–S–H phases).

(Androniuk et al., 2017) investigated the sorption of gluconate on C–S–H phases by combining wet-chemistry sorption studies and molecular dynamics simulations and reported R_d values of 4.5, 27, 217 dm^3·kg^{-1} for the uptake by C–S–H with Ca/Si of 0.83, 1.0 and 1.4, respectively. A fast sorption kinetics was observed and interpreted in terms of surface sorption rather than incorporation into the C–S–H structure. Based on molecular dynamics calculations, Androniuk and co-workers proposed that the sorption of gluconate is triggered by the formation of Ca-gluconate surface complexes on C–S–H. These results evidence the key role of Ca in the gluconate retention process, in line with experimental sorption trends reported for the uptake by C–S–H phases with increasing Ca/Si ratio (Androniuk et al., 2017; Nalet and Nonat, 2016). C–S–H phases with high Ca/Si ratios (Ca/Si > 1), have a positive apparent surface charge due to Ca^{2+} uptake, which overcompensates the negative surface charge of C–S–H caused by deprotonated silanol groups (Haas and Nonat, 2015; Labbez et al., 2011). Therefore, (Nalet and Nonat, 2016) interpreted the gluconate sorption to occur through interaction with Ca ions at the surface of the C–S–H particles. Speciation calculations showed that the increase of Ca/Si in C–S–H also leads to the formation of polynuclear aqueous Ca-gluconate complexes such as $CaGLUOH^0$, $Ca_3GLU_2(OH)_4^0$ or $Ca_2GLU_2(OH)_4^{2-}$, which lower the fraction of free Ca^{2+} at higher gluconate concentrations (Bouzouaid et al., 2021, 2022; Kutus et al., 2020). Due to the formation of strong aqueous Ca-gluconate complexes, the total concentration of Ca in the aqueous phase increases with the increase of the gluconate concentration. Depending on the experimental conditions, the formation of aqueous Ca-GLU complexes can lead to the desorption of calcium ions from the C–S–H surface, thus resulting in a decalcification of the C–S–H phases and accordingly in a weaker uptake of gluconate. In the aqueous phase, (Bouzouaid et al., 2022) proposed also the formation of the quaternary complex $Ca_3Glu_2(H_3SiO_4)_2(OH)_2^0$, which becomes relevant in the pore water of C–S–H systems with 0.9 < Ca/Si < 1.2 and prevailing over other Si-complexes (H_4SiO_4, $H_4SiO_4^-$, $H_2SiO_4^{2-}$). The consideration of such complexes is important for the accurate description of the solution chemistry in cementitious systems containing gluconate.

This study aims at quantitatively characterizing the uptake of gluconate and formate by cement hydrates (C–S–H, monocarbonate, hemicarbonate, monosulfate, ettringite) and PC, comparing the retention of both organic ligands, as well as providing new insights into the retention mechanism and the impact of these organic ligands on the structure and composition of the investigated cement phases. Following a similar approach as reported in (Guidone et al., 2024) for citrate, the uptake of formate and gluconate was investigated by characterizing both solid and liquid phases. Thermodynamic modelling was considered to derive solubility constants of formate and gluconate AFm-phases and to assess the aqueous speciation of formate and gluconate in the investigated systems.

2. Materials and method

2.1. Materials

Sulfate-ettringite (labelled as SO_4-AFt), AFm phases, monosulfate (Ms), monocarbonate (Mc) and hemicarbonate (Hc), and C–S–H phases were synthesized by the co-precipitation method. C_3A ($3CaO\ Al_2O_3$) was used as reactive precursor for the AFm phases. The C_3A and CA ($CaAl_2O_4$) were prepared from $CaCO_3$ (Merck Millipore, ≥ 98.5) and Al_2O_3 (Sigma-Aldrich, ≥ 99.0%) mixed for 1 day at a 3:1 or 1:1 M ratio and heated for 1 h at 800 °C, 4 h at 1000 °C and 24 h at 1425 °C (Nedyalkova et al., 2019). CaO was obtained by heating $CaCO_3$ (Merck, Supelco, ≥ 99.0%) at 1000 °C for 12 h and cooling it down in a closed desiccator to minimise the CO_2 uptake. Freshly prepared CaO was used for the synthesis of Hc and C–S–H phases. Ms, Mc, Hc, SO_4-AFt and C–S–H phases were synthesized with a solid to liquid, S/L, ratio of 44, 46, 44, 42 and 55 g·dm^{-3}, respectively.

Ms was prepared by mixing $CaSO_4{\cdot}2H_2O$ (Sigma-Aldrich, ≥ 97.0%) and C_3A with a stoichiometric ratio 1:1. Mc and Hc was synthesized by mixing C_3A, $CaCO_3$ and CaO with 1:1:0 and 1:$^1/_2$: $^1/_2$ stoichiometric ratio. SO_4-AFt was synthesized by mixing CaO and $Al_2SO_4{\cdot}16.3H_2O$ (Sigma-Aldrich, ≥ 60.0%) at a molar ratio of 6:1 in Milli-Q water. C–S–H phases were synthesized by mixing CaO and SiO_2 (Areosil 200, Evonik) in stoichiometric amounts with Milli-Q water, in order to achieve Ca/Si ratios of 0.8, 1,0, 1.2 and 1.4. All sample manipulations were performed under N_2 atmosphere in a glovebox. Ultra-pure water (Millipore, 18.2 MΩ) was used for both solution preparation and synthesis of cement phases.

Gluconate-AFm (S/L = 76.3 g·dm^{-3}) and gluconate-AFt (S/L = 104.8 g·dm^{-3}) were synthesized by mixing C_3A, CaO and Na-gluconate ($NaC_6H_{11}O_7$, Sigma-Aldrich, ≥ 98.0%) at a stoichiometric ratio of 1:1:2 and 1:3:6. The synthesis of formate-AFm (S/L = 46.2 g·dm^{-3}) and formate-AFt (S/L = 50.8 g·dm^{-3}) was carried out by mixing C_3A, CaO and Na-formate ($NaCHO_2$, Sigma-Aldrich, ≥ 99.0%) with a stoichiometric ratio of 1:1:4 and 1:3:6, respectively. An additional formate containing AFm phase (FOR-AFm_2) was prepared by mixing 1.26 g of CA, 1.79 g of CaO and 0.68 g of Na-formate (S/L = 83 g·dm^{-3}). Formate-AFm_2 was equilibrated for 84 days, gluconate-AFm, gluconate-AFt, formate-AFm, and formate-AFt for 60 days.

Ms, Mc, Hc, SO_4-AFt and C–S–H phases were equilibrated in a climatic room at 20 °C for 1 month under continuous shaking at 100 rpm, while gluconate(formate)-AFm and gluconate(formate)-AFt phases were equilibrated for 2 months. Phase separation was achieved through vacuum filtration using 0.45 μm nylon filters. Afterwards, the AFm phases and SO_4-AFt were dried over a saturated $CaCl_2$ solution at ~37 % relative humidity as detailed in (Guidone et al., 2024; Nedyalkova et al., 2019). Sorption experiments in the gluconate-containing systems

resulted in the formation of a gel-like phase (most likely made of Ca-gluconate complexes). The gel-like phase hindered phase separation, preventing in some cases the collection of sufficient volume for the quantification of the sorbed gluconate. C–S–H phases were dried under liquid nitrogen in a freeze dryer for 7 days following the procedure established by L'Hôpital et al. to minimise CO_2 uptake (L'Hôpital et al., 2015). The resulting dry solids were stored over saturated $CaCl_2$ solutions before further analysis.

Hydrated Portland cement (PC, CEM 42.5 N) was prepared by mixing 1 kg of dry cement with 400 g of Milli-Q water resulting in a water to cement ratio (w/c) of 0.4. The paste was hydrated for 28 days at 20 °C in closed polyethylene (PE) bottles. A part of the hydrated paste was ground by hand with an agate mortar to ≤ 63 μm without hydration stoppage to avoid contamination by organics, and used for sorption experiments with Na-formate and Na-gluconate. Further details about the composition and quantitative analysis of PC used in this study are reported in (Guidone et al., 2024).

2.2. Kinetic sorption experiments

The sorption kinetics of gluconate on cement hydrates was investigated between 1 day and 14 days. Kinetic studies were carried out by adding to the pre-synthesized phases suspensions 0.218 g of Na-gluconate, 9 cm^3 of NaOH solution ([NaOH] = 1 M) and 1 cm^3 of Milli-Q water. The addition of solution to suspensions avoided any drying of the synthesized solids before the sorption studies. This resulted in a total initial gluconate concentration of $[GLU]_{tot,in} = 21$ mM, a total initial Na concentration of $[Na]_{tot,in} = 0.2$ M and a total volume of 50 cm^3. Following the same approach, 10 cm^3 of 1 M Na-formate solution was added on the pre-equilibrated hydrate or cement suspensions targeting a total initial formate concentration of $[FOR]_{tot,in} = 221$ mM.

Suspensions were shaken continuously (100 rpm) at 20 °C, and sampled after selected contact times (t_{eq} (days) = 1, 2, 4, 7, 14). The solid and liquid phase were separated following the methodology reported in section 2.1. AFm phases and SO_4-ettringite were dried in a desiccator over saturated $CaCl_2$ solution (~35% relative humidity) at room temperature for 4 weeks. The C–S–H phases were freeze-dried using liquid nitrogen to minimise carbonation and kept under vacuum for 7 days to remove free water. Afterwards, C–S–H phases were also placed in a desiccator over saturated $CaCl_2$ solution and stored before further analysis.

2.3. Sorption experiments

Sorption experiments were carried out on pre-synthesized suspensions of cement phases and hydrated cements ($d_{particle} \leq 63$ μm) by adding different volumes (0.05–2.5 cm^3) of 1 M of Na-gluconate or 0.02–0.22 g of Na-gluconate corresponding to gluconate concentrations of $2.0{\cdot}10^{-5}$ M < $[GLU]_{tot,in}$ < $2.1{\cdot}10^{-2}$ M. In addition, 1 M NaOH solution was added to obtain in all cases a total sodium concentration $[Na]_{tot} = 0.2$ M and a pH = 13.3 and to be able to compare the sorption at comparable pH values. The uptake of formate was investigated in the concentration range of $2.0{\cdot}10^{-4}$ M < $[FOR]_{tot,in}$ < $2.2{\cdot}10^{-1}$ M by adding a total volume of 10 cm^3 containing various amounts of 1 M of Na-formate and 1 M of NaOH solutions to obtain a total sodium concentration of $[Na]_{tot} = 0.2$ M. The addition of the above-mentioned solutions led to an increased aqueous volume, thus resulting in suspensions of monosulfate, monocarbonate, hemicarbonate, sulfate-ettringite and C–S–H phase with a final S/L ratio of 44 $g{\cdot}dm^{-3}$, 37 $g{\cdot}dm^{-3}$, 35 $g{\cdot}dm^{-3}$, 32 $g{\cdot}dm^{-3}$ and 44 $g{\cdot}dm^{-3}$, respectively. In the case of sorption experiments with PC, 40 cm^3 of Milli-Q was added to 2.5 g of hydrated cement to achieve a S/L ratio of 50 $g{\cdot}dm^{-3}$.

The samples were equilibrated at 20 °C on horizontal shakers (100 rpm) for 7 days. Relatively short contacting times were chosen to minimise possible re-crystallization and precipitation processes as done previously by (Guidone et al., 2024; Nedyalkova et al., 2022). Phase separation was achieved by vacuum filtration through 0.45 μm nylon filters under inert atmosphere (N_2). Filtration was carried out without any washing steps to preserve the integrity of the solid phase. Drying was performed as described in section 2.1.

The uptake of gluconate and formate on the pre-synthesized cement phases was quantified in terms of the distribution coefficient, R_d, by using the following equation (Eq. 1):

$$R_d = \frac{C_{i,0} - C_{i,eq}}{C_{i,eq}} \cdot \frac{V}{m} \left[dm^3 \cdot kg^{-1}\right] \quad (1)$$

Where $C_{i,eq}$ represents the equilibrium concentration [mol·dm^{-3}] of gluconate or formate, $C_{i,0}$ the initial concentration [mol·dm^{-3}] added to the system, m is the mass [kg] of sorbent (e.g. PC, C–S–H phases, AFm phases) and V is the total volume [dm^3] of solution.

2.4. Solid phase characterization

After drying, solid samples were characterized by X-ray powder diffraction (XRD), thermogravimetric analysis (TGA) and infrared spectrometry (FT-IR). XRD analyses of AFm phases, sulfate-ettringite and PC were performed with a Panalytical X'Pert Pro MPD diffractometer with θ-θ geometry, using CuKα (λ = 1.54184 Å) radiation obtained using a Ge (111) Johansson monochromator and equipped with a solid state X-Celerator detector. XRD patterns were recorded at room temperature at a step size of 0.017° 2θ and a total measurement time of 45 min in the interval 5° < 2θ < 70°. The XRD patterns of the C–S–H phases, were analyzed with a CuKα1.2 radiation and the PIXcel detector was used. A 2θ interval of 5°–70°, a step size of 0.013° 2θ and a total measurement time of 1 h were applied at room temperature.

Infrared spectroscopy (FT-IR) analysis was carried out on Bruker Tensor 27 FT-IR spectrometer. Spectra were recorded in the wavelength range 4000 cm^{-1} - 400 cm^{-1} with a resolution of 4 cm^{-1}. This analysis was performed on powder samples in order to evaluate the possible incorporation or uptake of gluconate or formate.

TGA measurements were carried out on a Mettler Toledo TGA/SDTA 851 instrument (Mettler Toledo, Switzerland) to determine the amount of water bound and the amount of portlandite. Measurements were performed with ~30 mg of sample using a heating rate of 20 °C/min and a temperature range between 30 °C and 980 °C under N_2 atmosphere. Portlandite (CH) was quantified based on the weight loss in the temperature range 400–500 °C using the tangential method as detailed in (Lothenbach et al., 2016). The water losses and the amount of CH was expressed relative to the mass of the samples at 600 °C.

2.5. Liquid phase characterization

An aliquot of the supernatant solution was used for the pH determination. The pH measurement was performed using a Knick pH-meter with a SE 100 pH/Pt 1000 electrode at room temperature. The instrument was calibrated with NaOH solution of known concentrations (0.1, 0.2, 0.5 and 1 M) to minimise the alkali error (Traynor et al., 2020).

The characterization of the aqueous phase was performed by inductively coupled plasma-optical emission spectroscopy (ICP-OES) analysis. Total concentrations of Al, Ca, Na, Si and S were measured on an Agilent 5110 ICP-OES apparatus equipped with Agilent SPS 4 autosampler. Prior to each series, the instrument was calibrated using elemental standards at 5 different concentrations in the range 0.5–50 ppm. Ar is used as inert carrier gas. All samples were diluted in 2 wt% HNO3 with dilution factors of 10, 100 and 1000.

The total organic concentration was measured using a Sievers 5310 C total organic carbon (TOC) analyser using potassium hydrogen phthalate standards with 5 different concentrations in the range 1–50 ppm. Samples with expected low organic concentration were diluted by a factor of 5 with 0.1 M HCl solution, while samples with higher gluconate concentrations were diluted by a factor of 10, 100 and 1000 with 0.01 M

HCl solution. Results were given after subtracting the background concentrations measured in blank solutions. The electroneutrality of the solution has been checked for all system investigated considering the measured concentrations and pH values. In general, the values were in the expected ranges, although on average a 10% surplus of cations was observed, which was assigned to the uncertainties associated with the alkali concentration, the measured organic concentration as well as on the uncertainty associated to the pH measurement.

2.6. Thermodynamic calculations

Solubility products of the formate-AFm(AFt) and gluconate-AFm (AFt) solid phased synthesized in this work were determined on the basis of the measured total ion concentrations. The thermodynamic modelling program GEM-Selektor (GEMS) (Wagner et al., 2012) was used to calculate the activity of aqueous species, which takes into account chemical interactions involving solids, solid solutions, metal ions, and aqueous electrolyte at once. General thermodynamic data were taken from the PSI Nagra database, data for cement hydrates from the Cemdata18 database (Lothenbach et al., 2019). The CSHQ model (Kulik, 2011; Lothenbach et al., 2019) was used to describe the alkali uptake and the composition of C–S–H. In addition, the complexation of formate and gluconate with the different cations was considered using different complex formation constants as detailed in Table 1.

Table 1
Thermodynamic data used for thermodynamic calculations for the gluconate (Glu^- = gluconate) and formate (For^- = formate) system.

Species	Reaction	log $\beta^0_{m,l}$	Reference
Aqueous complexes			
$HGlu^0$	$H^+ + Glu^- \leftrightarrows HGlu^0$	3.64	Pallagi et al. (2010)[a]
$CaGlu^+$	$Ca^{2+} + Glu^- \leftrightarrows CaGlu^+$	1.56	Kutus et al. (2020)[a]
$Ca(Glu)_2^0$	$Ca^{2+} + 2Glu^- \leftrightarrows Ca(Glu)_2^0$	2.85	Bouzouaid et al. (2021)
$CaGluOH^0$	$Ca^{2+} + Glu^- + OH^- \leftrightarrows CaGluOH^0$	3.95	Bouzouaid et al. (2021)
$Ca_2Glu(OH)_3^0$	$2Ca^{2+} + 2Glu^- + 4OH^- \leftrightarrows Ca_2Glu_2(OH)_4^{2-}$	11.25	Bouzouaid et al. (2021)
$Ca_3Glu_2(OH)_4^0$	$3Ca^{2+} + 2Glu^- + 4OH^- \leftrightarrows Ca_3Glu_2(OH)_4^0$	16.10	Bouzouaid et al. (2021)
$HFor^0$	$H^+ + For^- \leftrightarrows HFor^0$	3.75	Calculated from $\Delta_fG°$ data by (Shock, 1995; Wieland et al., 2014)
$CaFor^+$	$Ca^{2+} + For^- \leftrightarrows Ca(For)^+$	1.43	Calculated from $\Delta_fG°$ data by (Shock, 1995; Wieland et al., 2014)
$Ca(For)_2^0$	$Ca^{2+} + 2For^- \leftrightarrows Ca(For)_2^0$	2.30	Calculated from $\Delta_fG°$ data by (Shock, 1995; Wieland et al., 2014)
$K(For)_2^-$	$K^+ + 2For^- \leftrightarrows K(For)_2^-$	−0.27	Calculated from $\Delta_fG°$ data by (Shock, 1995; Wieland et al., 2014)
$KFor^0$	$K^+ + For^- \leftrightarrows KFor^0$	0.03	Calculated from $\Delta_fG°$ data by (Shock, 1995; Wieland et al., 2014)
$Na(For)_2^-$	$Na^+ + 2For^- \leftrightarrows Na(For)_2^-$	−0.23	Calculated from $\Delta_fG°$ data by (Shock, 1995; Wieland et al., 2014)
$NaFor^0$	$Na^+ + For^- \leftrightarrows NaFor^0$	0.05	Calculated from $\Delta_fG°$ data by (Shock, 1995; Wieland et al., 2014)
Solids			
$Ca(Glu)_2$	$Ca^{2+} + 2Glu^- \leftrightarrows Ca(Glu)_2$	−4.19	Tits et al. (2002)
$Ca(For)_2$ (formicaite)	$CaFor_2 \leftrightarrows Ca^{2+} + 2For^-$	not available[b]	

[a] Values extrapolated to 0 M ionic strength using the WATEQ Debye-Hückel equation from those reported in (Kutus et al., 2020; Pallagi et al., 2010) by (Bouzouaid et al., 2021).

[b] (Lumsden, 1902) reports a high solubility of $Ca(HCOO)_2$ of 166 g·dm^{-3} at 20 °C.

Activity coefficients of the aqueous species were calculated with the built-in extended Debye-Hückel equation (Eq. 2) and NaOH as a background electrolyte:

$$\log \gamma_i = \frac{-A_y z_i^2 \sqrt{I}}{1 + B_y a \sqrt{I}} + bI \quad (2)$$

z_i is the charge of species i, I the effective molal ionic strength, a corresponds to 3.31, and b to 0.98 for NaOH electrolyte (Helgeson et al., 1981; Kulik et al., 2013). A_y and B_y are P,T-dependent Debye-Hückel solvent parameters.

The solubility products and saturation indices were calculated from the activity of the species Ca^{2+}, $Al(OH)_4^-$, OH^-, SO_4^{2-}, CO_3^{2-}, CHO_2^-, $C_6H_{11}O_7^-$ and H_2O, obtained using GEMS and the measured total concentrations.

3. Results and discussions

3.1. Uptake of formate and gluconate by AFm and AFt phases

3.1.1. Synthesis of formate and gluconate AFm and AFt phases

AFm phases consist of positively charged main layers with a general composition $[Ca_4Al_2(OH)_{12}]^{2+}$, and anions and water present in the interlayer region $[X_x{\cdot}nH_2O]^{2-}$. The interlayer can contain either two monovalent ($2X^-$) or one bivalent (X^{2-}) anion, while the amount of water (nH_2O) depends on the type of anion, temperature, and relative humidity (Buttler et al., 1959; Taylor, 1973). AFm phases form hexagonal or pseudo hexagonal crystals: monosulfate (Ms) and hemicarbonate (Hc) have a trigonal geometry (Kuzel and Pöllmann, 1991; Pöllmann et al., 1997), while monocarbonate (Mc) has a triclinic symmetry (François et al., 1998). The spectra of the ligand-free phases indicate the formation of $Ca_4Al_2(SO_4)(OH)_{12}{\cdot}6H_2O$ (C_4AsH_{12}) and traces of C_4AsH_{14} ($Ca_4Al_2(SO_4)(OH)_{12}{\cdot}8H_2O$) for the Ms samples, of hemicarbonate: $Ca_4Al_2(CO_3)_{0.5}(OH)_{13}{\cdot}5.5H_2O$ ($C_4Ac_{0.5}H_{12}$) as well as of some carbonated hemicarbonate, $C_4Ac_{0.8}H_{10.2}$ for the Hc sample and of monocarbonate: $Ca_4Al_2CO_3(OH)_{12}{\cdot}5H_2O$ (C_4AcH_{11})) as detailed in (Guidone et al., 2024). The XRD spectra of gluconate and formate containing AFm phases are shown in Fig. 1. Interestingly, both formate and gluconate–AFm are relatively well crystalline, in contrast to citrate–AFm ($Ca_4Al_2(C_6H_5O_7)_{0.67}(OH)_{12}{\cdot}6H_2O$), which showed a relatively broad basal spacing (Guidone et al., 2024).

The XRD of FOR-AFm (Fig. 1a) indicates the formation of a well-crystalline layered structure with high intensity bands at 10.9° and at 21.8° 2θ corresponding to the interlayer distances (003) and (006), respectively. In agreement with the study of (Pöllman, 1989) a d-spacing of 8.1 Å was obtained for formate-AFm, $Ca_4Al_2(HCO_2)_2(OH)_{12}{\cdot}5H_2O$. A main layer reflection (110) at 31.0° 2θ is observed as characteristic for AFm-phases with trigonal geometry such as Ms or Hc (Allmann, 1977). In addition, traces of portlandite were detected (reflection at ≈ 18° 2θ). The shoulder observed at 11.2° 2θ (7.9 Å) indicates the presence of a second formate AFm, possible with less water. The two peaks are better resolved at 21.8° 2θ (4.07 Å) and at 22.4° 2θ (3.97 Å).

The XRD of GLU-AFm, shown in Fig. 1b, also indicates the formation of typical layered structures of AFm phases. The main reflection at ≈ 8.5° 2θ indicates a larger basal distance of 10.3 Å for GLU-AFm than observed for FOR-AFm, in agreement with the larger size of gluconate ($H_{11}C_6O_7^-$) than formate (HCO_2^-). An increase of the interlayer distance can be expected for larger anions, as previously observed for different organic-containing AFm and LDH phases (Meyn et al., 1990; Okoronkwo et al., 2018; Von Hoessle et al., 2015; Wang et al., 2018). The corresponding 006 reflection of GLU-AFm at ≈ 17.1° 2θ ($d_{spacing}$ = 5.1 Å) partially overlaps with the main reflection of katoite ($Ca_3Al_2(OH)_{12}$), which is present in minor quantities. The broad signal at ≈ 32° 2θ corresponds to the main layer, 110, reflection of AFm phases. The presence

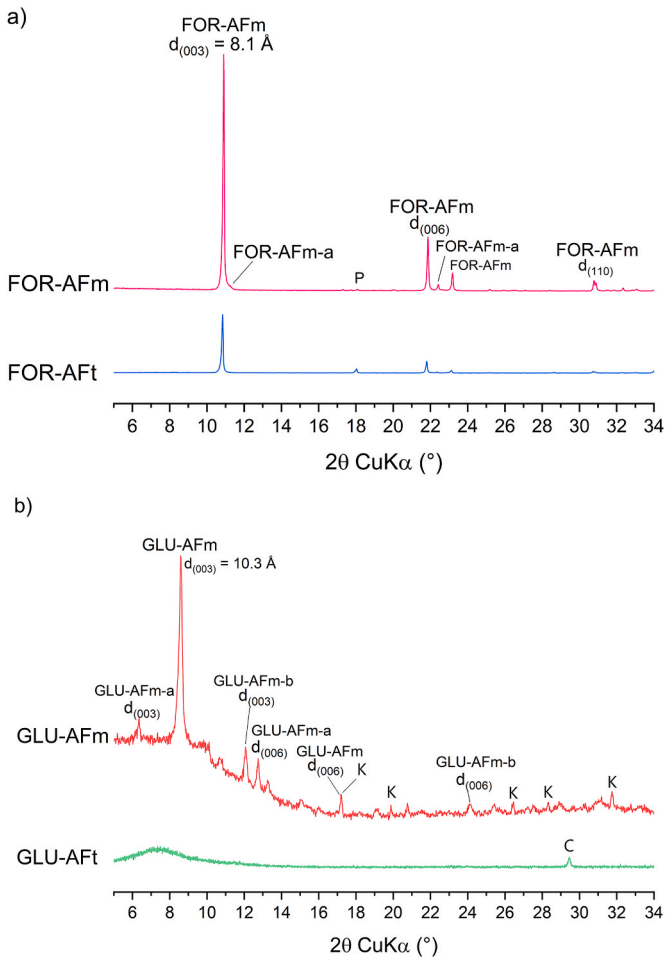

Fig. 1. XRD diffraction patterns of the synthesized samples: a) formate-AFm and formate-AFt, and b) gluconate-AFm and gluconate-AFt after 2 months of equilibration time. C: calcite; FOR-AFm: formate-AFm; GLU-AFm: gluconate-AFm; K: katoite ($Ca_3Al_2(OH)_{12}$); P: portlandite ($Ca(OH)_2$).

of katoite indicates a low stability of gluconate AFm phase. In addition to the main gluconate-AFm (GLU-AFm) signal, also two additional, smaller, signals at 6.3° 2θ (13.9 Å) and 12.1° 2θ (7.3 Å) are visible. Based on their narrow shape and their positions it was assumed that they correspond to the basal distance (labelled as d_{003}) of gluconate AFm phases with more (GLU-AFm-a) and less water (GLU-AFm-b). Many of the AFm phases have the tendency to show several basal spacing depending on drying and the activity of water as discussed in detail in (Baquerizo et al., 2015). The corresponding d_{006} signals are visible at 12.7° 2θ (6.9 Å) and at 24.1° 2θ (3.68 Å), respectively, which agrees with the assignment of those smaller peaks to AFm phases. The FT-IR spectra of those synthesis are summarised in ESM (Section 1 and 2).

The XRD (in Fig. 1a) and FT-IR data (shown in ESM) of the sample FOR-AFt sample is characterized by the same signals as detected for formate-AFm, which indicates that no formate-containing ettringite was formed but only formate-containing AFm phases. This is in agreement with observation for other monovalent anions such as chloride or iodide (Aimoz et al., 2012; Balonis et al., 2010), where also only AFm phases form, while the formation of ettringite is mainly observed for bi- and trivalent anions such as sulfate, chromate, selenite or citrate (Baur and Johnson, 2003; Guidone et al., 2024; Leisinger et al., 2010; Perkins and Palmer, 2000). In contrast to a previous study by (Dalconi et al., 2021), no M-phase ($Ca_6(Al(OH)_6)_2(HCOO)_6(OH)_{12}$) was observed in this work for formate. The authors reported the main diffraction peaks of this phase at d-spacings of 6.87 Å, 5.19 Å, 4.86 Å and 4.14 Å, which converted to Cu-anode, corresponds to = 12.9°, 17.1°, 18.2° and 21.4° 2θ.

The XRD spectra of the sample GLU-AFt (Fig. 1b) indicates the absence of a gluconate-containing ettringite phase, the presence of an amorphous phase and traces of calcite.

The total concentrations measured for the different elements in the aqueous solution (see Table 2) were used to calculate the ion activity products (IAP) for formate- and gluconate-AFm. The calculated IAP of formate-AFm reported in Tables 2 and is comparable to the solubility product of chloride (−27.3) or nitrate (−28.7) containing AFm phases (Balonis et al., 2010, 2011; Lothenbach et al., 2019). The solubility product calculated for gluconate-AFm is higher than that of formate-AFm, as also evidenced by the high calcium and aluminium concentrations and the presence of some katoite.

3.2. Sorption experiments

3.2.1. Uptake kinetic of formate and gluconate on monocarbonate, hemicarbonate, monosulfate and ettringite

The uptake kinetics of formate and gluconate sorption on pre-synthesized monocarbonate, hemicarbonate, monosulfate and ettringite was investigated by adding a total formate concentration of 221 mM or a gluconate concentration of 21 mM, while the total sodium concentration was kept at 200 mM. The addition of gluconate lowered the pH value by about 0.1–0.3 pH units (see Tables S1–S4, in the Electronic Supplementary Material, ESM). Most of the formate added remained in solution, such that a decrease by 4 pH units was observed for ettringite (Table S13, ESM), by 2 pH units for Mc (Table S11, ESM) and ≈1 pH unit for Ms and Hc (Table S10 and S12, ESM). Note that the decrease of pH is directly related with the decreasing volume of NaOH solution added with increasing formate concentration to have in all suspensions a $[Na]_{tot} = 0.2$ M.

The uptake of formate and gluconate occurred mainly during the first day and increased only moderately between 1 and 7 days, to remain approximately constants afterwards. The solution compositions, reported in the electronic supplementary material (ESM), in Tables S1 and S2 for gluconate, and Tables S10 and S11 for formate, show that the

Table 2
Measured pH (measurement error ± 0.1 pH units), Na, K, Ca, Al, (measurement error ± 5 %) and formate and gluconate (measurement error ± 7%) content for formate-, and gluconate-AFm phases used to calculate the ionic activity products (IAP) at 20 °C.

Phases observed[a]	pH	Na	Ca	Al	FOR/ GLU	IAP[b]
[mM]						
Formate-AFm[c]: $Ca_4Al_2(CHO_2)_2(OH)_{12}\cdot 6H_2O \rightarrow 4Ca^{2+}+2Al(OH)_4^- +2(CHO_2)^-+4OH^-+6H_2O$						
FOR-AFm, P	13.3	415	3.4	0.25	262/-	−27.6
FOR-AFm, P	13.1	219	6.8	0.11	125/-	−28.0
FOR-AFm, P, K[d]	13.1	231	3.2	0.33	105/-	−27.6
FOR-AFm, P[e]	13.4	249	11.0	0.035	192/-	−28.2
Mean						−27.9 ± 0.5
Gluconate-AFm[f]: $Ca_4Al_2(C_6O_7H_{11})_2(OH)_{12}\cdot 6H_2O \rightarrow 4Ca^{2+}+2Al(OH)_4^- +2(C_6O_7H_{11})^-+4OH^-+6H_2O$						
GLU-AFm, K	13.1	182	42	42	-/33.1	−24.5
GLU-AFm, K	13.0	161	75	61	-/70.3	−23.9
Mean						−24.2 ± 1.0
Amorphous phase, C[g]	12.6	173	18	13	107	-

[a] C: calcite; FOR-AFm: formate-AFm; GLU-AFm: gluconate-AFm; K: katoite; P: portlandite.
[b] Ion activity product calculated in this study and two sided 95% confidence interval.
[c] d-spacing 8.13 Å, molar volume 280 $cm^3\ mol^{-1}$ (trigonal structure).
[d] Data collected from formate-AFm_2.
[e] Data collected from formate-AFt experiment.
[f] d-spacing 10.3 Å, molar volume 376 $cm^3\ mol^{-1}$ (trigonal structure).
[g] Data collected from gluconate-AFt experiment.

concentrations of calcium and aluminium tend to increase as a function of equilibration times for Ms and Mc. In all cases, no additional solids formed.

3.2.2. Aqueous concentrations in equilibrium with AFm phases and ettringite

The sorption experiments with increasing concentrations of gluconate show that gluconate increases the calcium and sulfate concentrations in the presence of monosulfate and ettringite, while the pH is somewhat lowered. The increase of the sulfate concentration in the presence of gluconate indicates a partial replacement of sulfate by gluconate, similarly to the observations obtained for citrate (Guidone et al., 2024). Gluconate also lowers the pH and increases the calcium concentration in solution, which is related to the formation of stable calcium gluconate complexes. Thermodynamic modelling using the data summarised in Table 1 indicates that aqueous Ca speciation at pH values above 12 is dominated by the ternary $CaGluOH^0$ and $Ca_3Glu_2(OH)_4^0$ complexes. This is in agreement with the findings previously reported by (Bouzouaid et al., 2022).

In the case of formate (see Tables S29–S31 in ESM), pH values and sulfate concentrations remain constant at formate additions below 100 mM, indicating a very low replacement of sulfate by formate. Also, the calcium concentrations do not vary significantly, which agrees with the weak complexation between Ca^{2+} and formate (see Table 1). This is further confirmed by thermodynamic scoping calculations, which showed that Ca^{2+} and $CaOH^+$ were the major aqueous Ca-species in solution below 100 mM formate. Calcium formate complexes, $CaFor^+$ and $Ca(For)_2^0$, become only important at formate concentrations well above 100 mM. For higher formate concentrations, the experimentally determined Ca concentrations increased, while the pH values decreased due to the high concentration of formate in solution indicating an only weak formate uptake.

Recent studies have shown that iodide, selenite, and selenite are sorbed in the inner and outer surface sites of hemicarbonate and monosulfate, while citrate is sorbed only in the case of hemicarbonate in both the inner and outer surface area (Guidone et al., 2024; Lothenbach et al., 2024; Nedyalkova et al., 2022). The sorption on monocarbonate was observed to be much lower and to occur on the outer surface area only, as interlayer sorption was suppressed by the rigid structure and narrow interlayer distance of monocarbonate (Guidone et al., 2024; Lothenbach et al., 2024; Nedyalkova et al., 2022). The total sorption capacity of AFm phases, i.e. the sum of surface and interlayer anion sorption sites, corresponds for single charged anions to 3.7 mol·kg^{-1} Mc, 3.2 mol·kg^{-1} Ms and 4.8 mol·kg^{-1} ettringite. The uptake of organics on the external surfaces of AFm phases has been observed to be approximately 200 times lower (Guidone et al., 2024), corresponding to ≈ 0.02 mol per kg solid.

Sorption isotherms for the uptake of gluconate and formate by AFm phases and ettringite are shown in Fig. 2. In the case of gluconate, only concentrations above 0.1 mM gluconate equilibrium concentration could be measured, and thus only limited sorption data are available for this system. Fig. 2a shows that gluconate sorbs moderately on hemicarbonate and ettringite, and weaker on monosulfate, which agrees with the sequence observed in previous sorption experiments (Lothenbach et al., 2024; Nedyalkova et al., 2022). The limited amount of sorption data for gluconate makes the interpretation difficult. However, the data tentatively indicate an uptake of gluconate in both outer surface and interlayer sites for hemicarbonate, while for monosulfate the uptake is potentially limited to the outer surface sites, as previously observed for citrate (Guidone et al., 2024). For ettringite, no steps at around 0.02 mol·kg^{-1} are visible, indicating potentially an uptake on both out surface sites as well as within the water containing channels of ettringite. For the uptake of gluconate an R_d value of (119 ± 75) dm^3·kg^{-1} was determined for Hc, a tentative value of (1.27 ± 0.72) dm^3·kg^{-1} for Mc bases on the kinetic experiments, of (30 ± 11) dm^3·kg^{-1} for Ms and (38 ± 38) dm^3·kg^{-1} for ettringite.

The uptake of formate by Mc, Hc and AFt is expectedly weak (R_d ~ 1–3 dm^3·kg^{-1}) (Wieland et al., 2016) due to the electrostatic forces occurring between cement phases and formate (Fig. 2b). R_d values of 1.5 ± 0.1 dm^3·kg^{-1}, 93 ± 93 dm^3·kg^{-1}, 2.3 ± 0.9 dm^3·kg^{-1} and 2.9 ± 1.4 dm^3·kg^{-1} were derived for Mc, Ms, Hc and ettringite, respectively, for low formate solution concentrations <2 mM. Except for the high values associated with a very high uncertainty observed for Ms, the R_d values for formate are comparable to the values reported by Wieland et al. (2016): $R_{d\ (Ms)} \approx 2$ dm^3·kg^{-1}, $R_{d\ (Mc)} \approx 0.3$ dm^3·kg^{-1}, $R_{d\ (AFt)} \approx 1$ dm^3·kg^{-1} and $R_{d\ (Hc)} \approx 20$ dm^3·kg^{-1} at ≈ 3 mM formate and lower pH values of ≈12. The comparable values also seem to indicate that in the case of ettringite and AFm phases, where anions compensate the positive charge of the main layer, the pH has a minor effect on the R_d values, with the exception of Hc, where formate competes with OH^- and a clearly lower uptake was observed in the present study at pH 13.2 than by Wieland et al. at pH ≈ 12.

3.2.3. Solid AFm phases and ettringite

A slight variation of the main basal spacing of Hc values is observed in the presence of gluconate and formate (Fig. 3). The interlayer

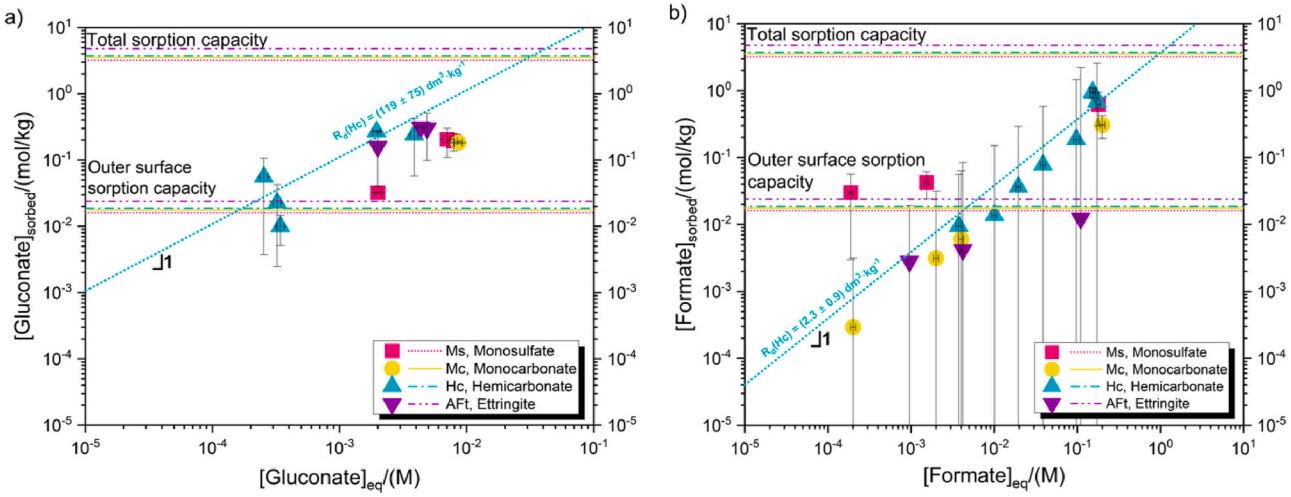

Fig. 2. Experimental a) gluconate and b) formate sorption isotherm for monosulfate (Ms), monocarbonate (Mc), hemicarbonate (Hc) and ettringite (AFt) after an equilibration time of 7 days. The upper and lower horizontal lines indicate the overall potential anion uptake and the uptake on the outer surface (1:200) (Guidone et al., 2024) of Ms, Mc and Hc, respectively.

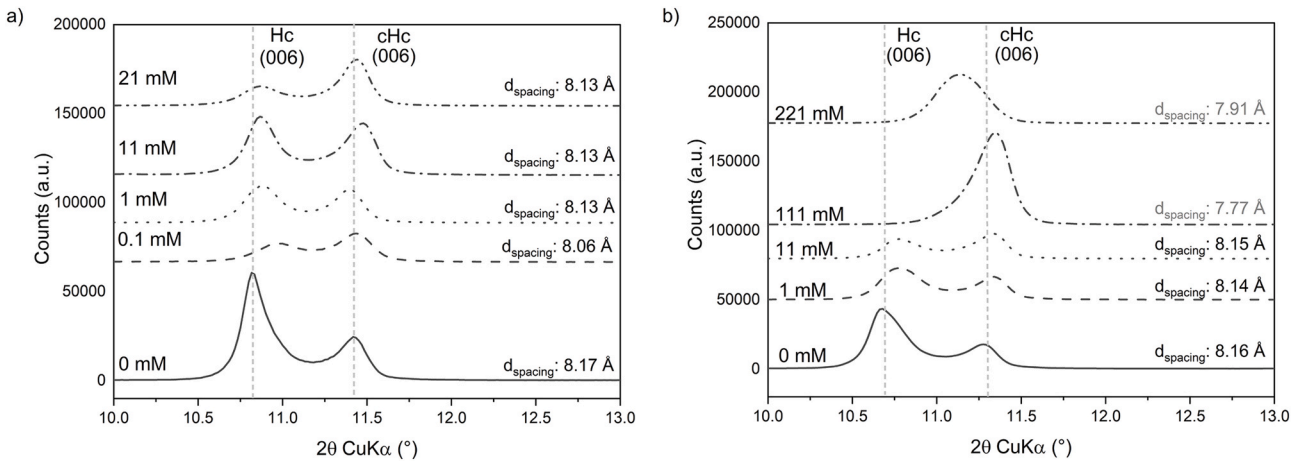

Fig. 3. XRD patterns of hemicarbonate after sorption of a) gluconate and b) formate (contacting time t = 7 days). Effect of gluconate/formate on the basal spacing of Hc (hemicarbonate) and cHc (carbonated hemicarbonate).

distances of both hemicarbonate (Hc) and carbonated hemicarbonate (cHc, $C_4Ac_{0.8}H_{10.2}$ (Runčevski et al., 2012)) shift to higher 2θ° values, indicating a small decrease in basal spacing with gluconate (Fig. 3). At low initial formate concentrations, no significant effect was observed. At intermediate formate concentration the relative intensity of the Hc signal decreases. At $[FOR]_{tot,in} \geq 111$ mM, only the reflection of cHc is present but shifted towards lower 2θ° values, while the signal of Hc is no longer visible, indicating a destabilisation of Hc. Furthermore, the decrease of the relative peak intensity with increasing gluconate and formate concentration may indicate a decrease in ordering of the stacking and/or a more variable interlayer distance. Note that the main layer signal at ≈ 31° 2θ, related to the 110 plane, did not broaden or decrease in intensity.

The XRD spectra (see Figs. S3, S4, S8 and S9 in the ESM), indicate a strong broadening of the main basal signal mainly for Ms, and to a lower extent for Mc, indicating again a disordering effect of gluconate on AFm phase and possibly fewer stacking layers in the c direction. The apparent slight shift of the basal spacing to lower 2θ° values is probably mainly related to the reduced number stacking layers in the c direction leading to an apparent shift of the basal reflection lower angles as discussed in detail in the literature (Grangeon et al., 2013; Mesecke et al., 2022). These findings are in agreement with the results obtained for the kinetic experiments series, where a broadening of the basal reflection was observed for Hc, but not for Mc, which is also in agreement with observations of Nedyalkova and co-workers (Nedyalkova et al., 2019). The ettringite phases (Figure S5 and S10, ESM) showed no significant changes.

The presence of gluconate increases the concentration of sulfate in solution for Ms and ettringite (see Table S18 and S21, ESM), which agrees with the observed uptake of gluconate on outer surface sites as suggested by (Ma et al., 2017) for monosulfate. The weak increase in sulfate concentration has been observed upon formate addition in the presence of ettringite (Table S32, ESM), while in the case of Ms, the sulfate concentration and the pH values decreased at higher formate concentrations.

3.3. Uptake of formate and gluconate by C–S–H phases

3.3.1. Uptakes kinetic of gluconate and formate on C–S–H phases

The uptake kinetics of both gluconate and formate on pre-synthesized C–S–H phases with Ca/Si = 0.8, 1.0, 1.2, and 1.4 as detailed in (Guidone et al., 2024), was investigated for equilibration times $1 \leq t_{eq}$ (days) ≤ 14. Total gluconate concentrations of up to 21 mM and formate concentrations of up to 221 mM were added to the C–S–H suspensions and the samples were further equilibrated under continuous shaking, prior to separation and analysis. The pH values remained almost constant for all gluconate samples (Tables S5–S8, in the ESM), but was lowered by ≈ 1 pH unit (Ca/Si ≥ 1.0) and up to of 3 pH units for C–S–H with a Ca/Si of 0.8 in the case of formate as less NaOH is added with the increase of formate concentration (see Tables S14–S17, in the ESM). The presence of high gluconate and formate concentrations clearly destabilizes the portlandite initially present in the C–S–H phases with Ca/Si = 1.2 and 1.4. The destabilisation of portlandite is related, in the case of gluconate, mainly due to the formation of the aqueous species Ca-gluconate complexes, $CaGluOH^0$, $Ca_2(Glu)_2(OH)_4^{2-}$ and $Ca_3(Glu)_2(OH)_4^0$, as shown also in the study of (Bouzouaid et al., 2022). In the case of formate, where the complex formation between Ca and formate is weak (see Table 1), little effect on the calcium concentration is observed, except for those samples with very high formate additions (111 and 221 mM), where the hydroxide concentration and thus the pH is lowered, resulting in higher calcium concentration in equilibrium with C–S–H (Yan et al., 2022) as well as in the destabilisation of portlandite (see Table S35 and S36, ESM).

In general, gluconate and formate solution concentrations decrease mainly during the first day, and show only moderate variations afterwards, indicating that again an equilibration time of 1 week is sufficient to investigate sorption.

3.3.2. Effect of gluconate and formate on C–S–H

A significant increase of Ca concentration takes place for all C–S–H phases with increasing gluconate concentration, in agreement with the observations reported in (Bouzouaid et al., 2022). The increase is particularly distinct for C–S–H with a Ca/Si = 1.0, where Ca concentrations increased from 0.2 mM in the absence of gluconate to 1.1 mM in the presence of 21 mM of gluconate, and less strong at higher Ca/Si as detailed in Tables S22–S25 (see ESM). The stronger increase of Ca at lower Ca/Si is related to the stronger decrease in pH observed with increasing gluconate concentration and the common ion effect of Ca, Si and hydroxide for C–S–H. The lower Na concentrations at low Ca/Si ratios indicate a strong uptake of Na^+ on the ion exchange sites of C–S–H phases as reported also e.g. by (Yan et al., 2022), as well as a lower sorption of gluconate, resulting in lower OH^- concentration in solution. This effect is less pronounced with the increase of Ca/Si ratio.

In the case of formate, a strong increase of Ca concentration is observed, in particular at lower Ca/Si, where the pH decreased strongly at higher formate concentrations (see Tables S33-S36, ESM). The strong effect of pH is in agreement with the trends reported in literature, where lower pH result in more Ca and less Si in solution as well as in a decalcification of C–S–H (L'Hôpital et al., 2015; Liu et al., 2021; Yan et al., 2022). The decrease of pH value is more pronounced for formate

than for gluconate (see Tables S33-S36, ESM).

Mass balance calculations indicate that only a slight decrease of the Ca content in C–S–H takes place at high gluconate and formate concentrations (see Tables S27 and S38 in the ESM), although the aqueous Ca concentration increased and any portlandite originally present at Ca/Si = 1.2 and 1.4 was dissolved. The presence of gluconate or formate has a negligible effect on the interplanar distance for C–S–H phases, although a peak broadening is observed in particular at higher Ca/Si, probably related to a decrease in the number of layers stacked in c-direction (Grangeon et al., 2013; Mesecke et al., 2022). The apparent decrease in basal spacing can be explained by the decrease in the number of stacked layers.

3.3.3. Gluconate and formate uptake by C–S–H

Fig. 4 shows the sorption isotherms for the uptake of gluconate and formate by C–S–H phases and PC. The quantification of C–S–H weight, calculated by combining mass balance calculation and water content obtained from TGA analysis, is reported in Table S26 and S37 (see the ESM file). For all C–S–H phases investigated, the uptake of gluconate shows a linear increase with increasing gluconate concentration in the aqueous phase. Gluconate sorbs relatively weakly on C–S–H phases with a Ca/Si = 0.8 and 1.0 with average R_d values of (1.9 ± 1.3) $dm^3 \cdot kg^{-1}$ and (7.0 ± 3.0) $dm^3 \cdot kg^{-1}$. For Ca/Si = 1.2 and 1.4 the sorption of gluconate is visibly stronger with average R_d values of (15.6 ± 2.5) $dm^3 \cdot kg^{-1}$ and (33.9 ± 17.5) $dm^3 \cdot kg^{-1}$, respectively.

The strong increase of uptake of gluconate at higher Ca/Si confirms earlier observations of (Androniuk et al., 2017; Bouzouaid et al., 2022; Nalet and Nonat, 2016), who reported that the uptake of gluconate is mediated by complexation with calcium at the surface of C–S–H phases. The R_d values measured here at pH of ≈ 13, are roughly a factor 10 lower than the R_d values of 4.5 $dm^3 \cdot kg^{-1}$ (Ca/Si = 0.83), 40 $dm^3 \cdot kg^{-1}$ (Ca/Si = 1) and 285 $dm^3 \cdot kg^{-1}$ (Ca/Si = 1.4) measured at pH values of 10.5–12.3 (Androniuk et al., 2017). The lower pH values in the experiments of (Androniuk et al., 2017) resulted in higher calcium concentrations of 1, 2 and 12 mM for Ca/Si = 0.83, 1.0 and 1.4, than observed here with 0.1, 0.2, 3 mM Ca for Ca/Si = 0.8, 1.0 and 1.4 at pH ≈ 13, underlining the important role of calcium (and thus indirectly of pH) on the ability of C–S–H to take up gluconate. It should be noted that the presence of 200 mM Na in all experiments presented here influences the formation of calcium gluconate complexes (Bouzouaid et al., 2021), the surface charge of C–S–H (L'Hôpital et al., 2015) and thus gluconate uptake by C–S–H.

Based on molecular dynamic calculations, (Androniuk et al., 2017) proposed the formation of Ca-gluconate surface complexes on C–S–H.

Fig. 4b shows the sorption isotherms calculated for the uptake of formate by C–S–H phases. Due to the small difference between the initial and the measured formate concentration, no uptake could be quantified for $[FOR]_{tot,in}$ = 11 mM for C–S–H phases with a Ca/Si = 0.8, 1.0 and for $[FOR]_{tot,in}$ = 4.4 mM for Ca/Si = 1.2 and 1.4. At low formate concentrations $[FOR]_{eq} < \sim 10^{-3}$ M, the uptake occurs on all C–S–H phases, increases linearly with the increase of formate concentration and is independent of the Ca/Si ratio of the C–S–H, in contrast to the observation for gluconate. This indicates that the uptake of formate by C–S–H is not related to calcium present at the surface of C–S–H, in agreement with the weak character of the Ca-formate complexes forming in the aqueous phase (Shock, 1995; Shock and Koretsky, 1995; Shock et al., 1997; Wieland, 2014) (Table 1). At $[FOR]_{eq} > \sim 10^{-2}$ M, due to the weak interaction of formate with C–S–H phases, no quantification of sorbed formate could be derived.

At formate concentration lower than 2 mM, average distribution coefficient R_d values of (25.6 ± 15.6) $dm^3 \cdot kg^{-1}$, (12.3 ± 5.0) $dm^3 \cdot kg^{-1}$, (12.5 ± 8.3) $dm^3 \cdot kg^{-1}$ and (34.4 ± 16.6) $dm^3 \cdot kg^{-1}$ for Ca/Si of 0.8, 1.0, 1.2 and 1.4 respectively were determined, which is considerably lower than the R_d values of 190 and 102 $dm^3 \cdot kg^{-1}$ determined by (Wieland et al., 2016) for low and high Ca/Si ratio, respectively. The lower uptake observed in the present study is probably related to the higher pH values present in our experiments (pH > 13), which increases the negative charge on C–S–H (L'Hôpital et al., 2015) and thus decreases anion sorption, compared to the experiments of (Wieland et al., 2016) at pH 10.5 to 12.5, where no additional NaOH had been added.

3.4. Gluconate and formate sorption on Portland cement

The uptake of gluconate by hydrated Portland cement paste increases linearly with the increase of gluconate concentration as shown in Fig. 4a; solution composition is detailed in Table S28, in the ESM file. The measured uptake of gluconate on Portland cement is with an average R_d of (131 ± 10) $dm^3 \cdot kg^{-1}$ significantly higher than the sorption on C–S–H, monosulphate and ettringite measured here at pH 13, but in the same range as the 285 $dm^3 \cdot kg^{-1}$ measured at pH values of 12.3 for Ca/Si = 1.4 (Androniuk et al., 2017) as illustrated in Fig. 5. The strong increase of gluconate uptake on C–S–H with the calcium concentration in solution explains the relatively high sorption measured on PC (and that gluconate sorbs strongly on C–S–H phases with high Ca/Si). Gluconate also sorbs on portlandite with an average $R_d \sim 22$ $dm^3 \cdot kg^{-1}$ at pH 12.5 calculated from the sorption measurements reported by (Nalet and Nonat 2016). Thus, the uptake on high Ca/Si C–S–H contributes significantly to the gluconate uptake on PC together with the uptake on

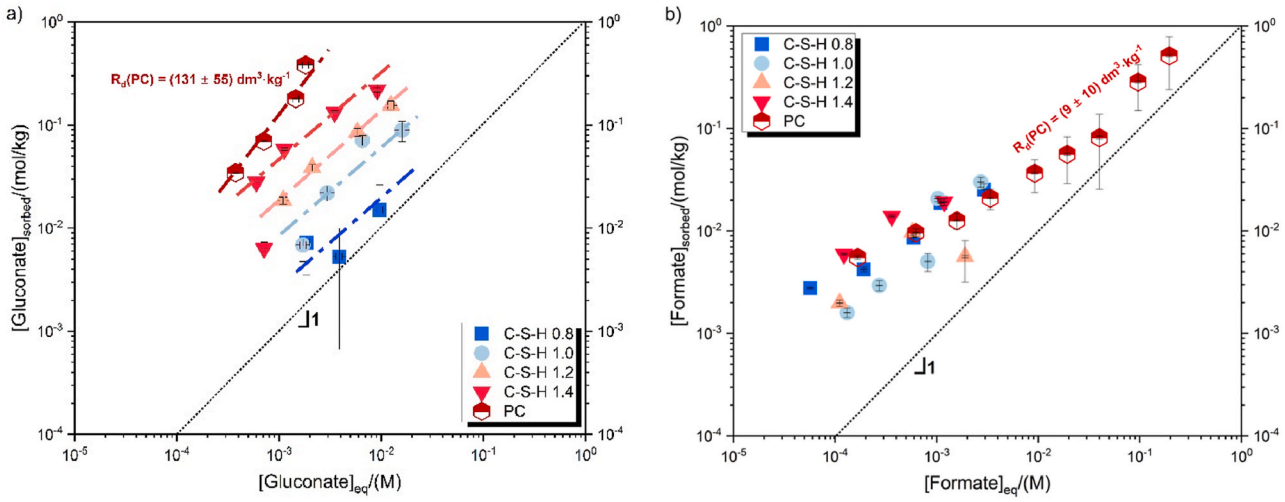

Fig. 4. Sorption isotherms calculated as moles of a) gluconate and b) formate, expressed per kg of solid phase, for C–S–H phases with a ratio of 0.8 ≤ Ca/Si ≤ 1.4 and Portland cement (PC) after 7 days of contacting time. The lines are intended as eye guide only.

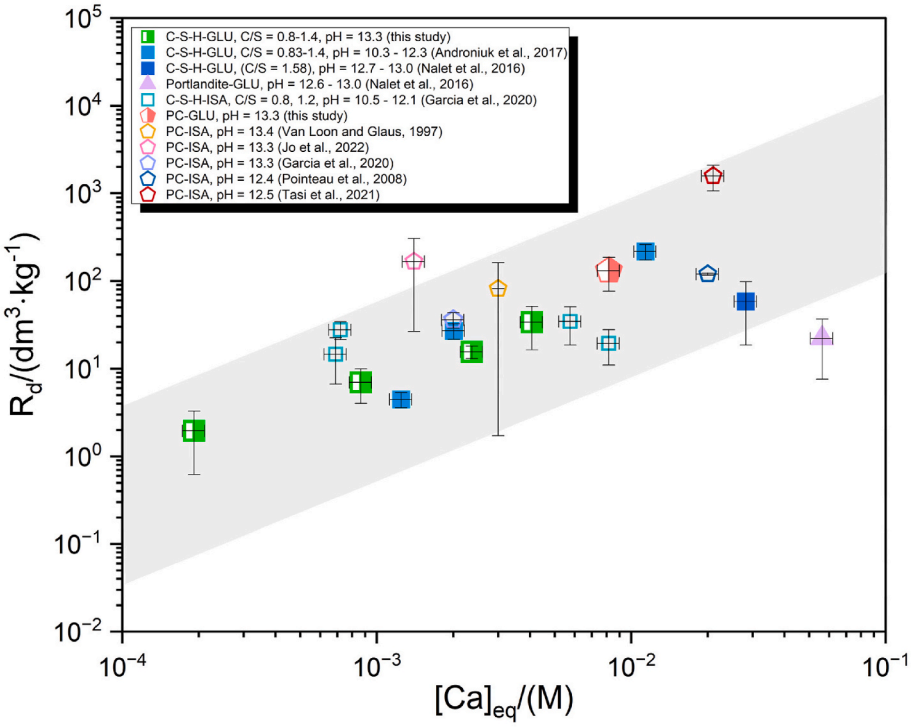

Fig. 5. Comparison of average R_d values for the uptake of gluconate (half-filled symbols) and α-ISA (empty symbols) on C–S–H phases, portlandite and PC, as a function of the Ca equilibrium concentration.

Hc and ettringite, while the contribution of portlandite is less important. Based on the strong dependency, a decrease of gluconate sorption at lower calcium concentrations was observed in Fig. 5, a somewhat lower R_d than measured here can be expected for hydrated Portland cements, where pH values of ≈13.5 and Ca concentrations in the range of 1–3 mM are generally observed (Vollpracht et al., 2016), while the R_d values might be higher in leached cements characterized by higher Ca concentrations in the pore solution.

Glaus and co-authors investigated the uptake of sodium gluconate ($[GLU]_{tot,in} = 10^{-7}$-10^{-4} M) on hydrated cement equilibrated with artificial cement pore water ($[Ca]_{tot} = 1.6{\cdot}10^{-3}$ M), corresponding to a $R_d \sim 1$ $dm^3{\cdot}kg^{-1}$ and $R_d \sim 10^5$ $dm^3{\cdot}kg^{-1}$ for the lowest ($[GLU]_{tot,in} = 10^{-7}$ M) and the highest ($[GLU]_{tot,in} = 10^{-4}$ M) total initial gluconate concentration, respectively (Glaus et al., 2006). The decrease in the R_d value with increasing GLU concentration, as observed by (Glaus et al., 2006), indicated non-linear sorption of GLU in the given concentration range.

Gluconic acid has chemically a strong similarity with α-isosaccharinic acid (α-ISA). R_d values determined in this work for gluconate are comparable with those reported in the literature for α-ISA. A $R_d \approx 120$ $dm^3{\cdot}kg^{-1}$ was reported for the uptake of α-ISA ($[\alpha\text{-ISA}]_{tot} = 8.5{\cdot}10^{-4}$ M) by degraded hardened cement paste (pH = 12.4, $[Ca]_{tot} \approx 10^{-2}$ M) over an equilibration time of 200 days (Pointeau et al., 2008). The authors observed a strong dependency between Ca concentration (and pH) with the uptake of α-ISA by cement. Hence, an increase of R_d from 4 $dm^3{\cdot}kg^{-1}$ to 100 $dm^3{\cdot}kg^{-1}$ was observed when the pH dropped from 13 to 12.5, with the consequent increase in Ca concentration by one order of magnitude. Given the fast equilibrium conditions reached within 3 days, Pointeau and co-workers proposed that α-ISA uptake is likely controlled mainly by surface complexation mechanism, mainly involving C–S–H phases (Pointeau et al., 2008).

García and co-workers studied the uptake of α-ISA by C–S–H phases with Ca/Si = 0.8 and 1.2 (pH = 10.5–12.1) as well as on hydrated cement (pH = 13.3) (García et al., 2020) again indicating a non-linear sorption of α-ISA in the given concentration range. Sorption data show the correlation between sorbed gluconate and Ca concentration in the aqueous phase. The higher α-ISA uptake on C–S–H 1.2 was interpreted in terms of Ca-α-ISA complex formation at the surface of C–S–H phase. Data were satisfactorily modelled using one-site Langumir isotherm. However, the same approach did not properly explain the sorption behaviour in the PC-α-ISA system. Sorption experiments conducted on hydrated cement resulted in an average R_d value of ≈40 $dm^3{\cdot}kg^{-1}$ at $[Ca]_{eq} \approx 2.0{\cdot}10^{-3}$ M.

A strong dependency of R_d values with the concentration of α-ISA ($R_d \approx 400$ $dm^3{\cdot}kg^{-1}$ for $[\alpha\text{-ISA}]_{tot} = 10^{-5}$ M and $R_d \approx 1$ $dm^3{\cdot}kg^{-1}$ for $[\alpha\text{-ISA}]_{in} = 0.3$ M) was observed by Van Loon and Glaus at pH 13.3 and $[Ca]_{tot} = 3$ mM (Van Loon and Glaus, 1998). Similar trend were observed in the study of (Jo et al., 2022) conducted on hydrated cement (S/L = 1 $g{\cdot}dm^{-3}$) in the α-ISA concentration range 10^{-5} M < $[\alpha\text{-ISA}]_{tot}$ < 10^{-2} M. The authors interpreted the uptake of α-ISA on hydrated cement using a one-site Langumir isotherm.

Tasi and co-workers investigated the uptake of α-ISA by PC in the degradation stage II (pH = 12.5, $[Ca]_{tot} = 21$ mM), and reported R_d values ranging from ≈ 200 $dm^3{\cdot}kg^{-1}$ (at S/L = 2 $g{\cdot}dm^{-3}$) to ≈ 1600 $dm^3{\cdot}kg^{-1}$ (at S/L = 50 $g{\cdot}dm^{-3}$) (Tasi et al., 2021). The strong uptake was interpreted in terms of affinity with Ca^{2+} ions on cement.

Fig. 5 underpins the evident correlation between the uptake of GLU/ISA (expressed in terms of R_d values) and the Ca concentration in the pore solution of the investigated PC or C–S–H system.

The uptake of formate on hydrated Portland cement paste increases linearly with the increase of formate concentration. For a formate equilibrium concentration below ≈ 10^{-3} M, the same uptake was observed as for the C–S–H phases as visible in Fig. 4b. The R_d of (8.6 ± 2.6) $dm^3{\cdot}kg^{-1}$ observed here on hydrated cement paste (pH ≈ 13.3), is somewhat higher than the R_d values of ≈ 1 $dm^3{\cdot}kg^{-1}$ determined by (Wieland et al., 2016) for hydrated cement pastes at a pH of 12.9. The lower R_d value observed by (Wieland et al., 2016) might be related to the higher S/L ratio used (i.e. 8622 $g{\cdot}dm^{-3}$) compared to the S/L ratio of 50 $g{\cdot}dm^{-3}$ used in this study. Another possible reason for the discrepancy of the R_d values is the experimental set-up: cement samples were mixed with a solution containing the aimed formate concentration, samples were let equilibrate at different times (t = 1 h, 28 d, 390 d), and the

aqueous formate concentration was measured in the squeezed solution (Wieland et al., 2016). It is worth of mentioning that (Wieland et al., 2016) were not able to quantify the uptake of ^{14}C-formate in the sorption batch experiments carried out on hydrated cement (S/L = 333 g·dm^{-3}). In agreement with (Wieland et al., 2016), Nedyalkova et al. (2021) obtained an R_d value of 0.9 dm^3·kg^{-1} on aged hydrated cement (S/L = 130 g·dm^{-3}) at pH = 13.4, which lower value can be due to the lower fraction of C–S–H phases estimated in the cement composition analysis.

3.5. Sorption of gluconate and formate in comparison with other organics

Gluconate, formate as well as citrate (Guidone et al., 2024) have been observed to sorb relatively strongly on hemicarbonate, while the uptake by monosulfate and monocarbonate was limited and occurred on outer-surfaces site mainly, as shown by the sorption isotherms for formate and gluconate in Fig. 2. Fig. 6 compares the R_d values for the uptake of formate, citrate and gluconate on AFm phases (Ms, Hc), AFt and PC. The uptake of gluconate and citrate on Hc is approximately 2 orders of magnitude higher than the uptake of formate, the same preference for gluconate over citrate and over formate was observed for ettringite. Conversely, Ms shows a higher affinity towards citrate uptake (Guidone et al., 2024), followed by formate and gluconate. The higher distribution ratio quantified for the Ms-FOR system might not be representative of the studied system, as it is based on a limited number of experimental data and a high error. If compared to the citrate and gluconate systems, no significant difference of the distribution coefficient can be observed for the uptake of formate by Hc and AFt. The uptake of gluconate and citrate by PC is comparable to each other, indicating a cumulative effect on the different phases present in PC in addition to a strong effect of Ca-concentration as discussed above and in (Guidone et al., 2024).

In the case of C–S–H phases, the uptake of gluconate and citrate is mediated by a Ca complex at the C–S–H surface (Androniuk et al., 2017; Guidone et al., 2024) and therefore is dependent on the Ca/Si of the solid phase (Fig. 7). For the strongly complexing ligands gluconate and citrate the uptake on C–S–H phases is increased in the presence of more calcium in solution as shown in Fig. 5 for gluconate and in (Guidone et al., 2024) for citrate. Thus, for both gluconate and citrate the sorption increases with the Ca/Si ratio of C–S–H and is even higher for PC, as shown in Fig. 7. Since the uptake of citrate and gluconate is increased in the presence of more calcium, the higher retention of gluconate and

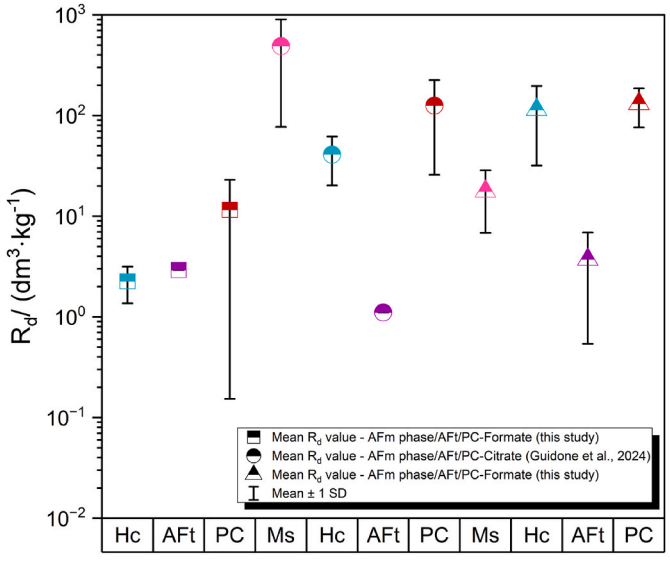

Fig. 6. Comparison of average R_d values collected for the uptake of formate (squares), citrate (Guidone et al., 2024) (circles) and gluconate (triangles) on AFm phases (Ms, Hc) and AFt at pH 13 and for a contacting time of 7 days.

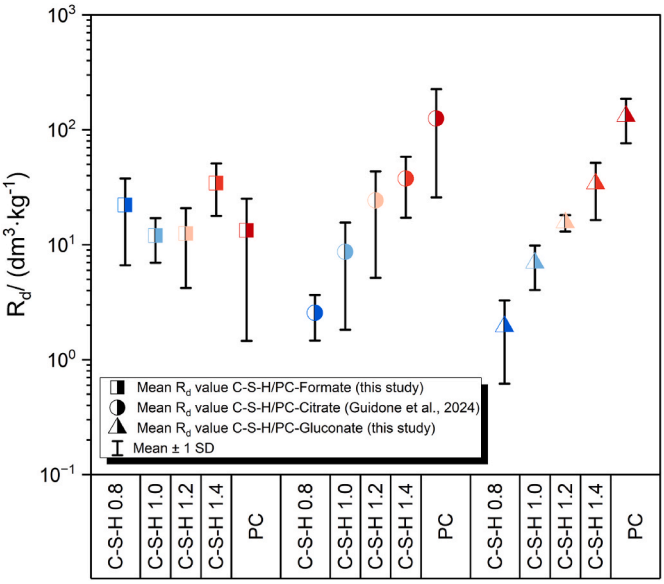

Fig. 7. Comparison of average R_d values collected for the uptake of formate (squares), citrate (Guidone et al., 2024) (circles), and gluconate (triangles) on C–S–H phases with a Ca/Si ratio of 0.8–1.4 and PC at pH 13 and for a contacting time of 7 days.

citrate on hydrated PC is mainly related to the higher availability of calcium in PC, where the presence of portlandite results in the formation of C–S–H with a Ca/Si in the range of 1.6–1.8 (Taylor et al., 2010) as well as in higher calcium concentration in solution (see Fig. 5 and sections 5.2, 5.3, 6.2 and 6.3 in ESM). In addition, not only C–S–H is present in hydrated PC, but also ettringite and AFm phases, which also contribute to the observed high uptake in hydrated PC.

This trend is not observed in the case of formate (Figs. 6 and 7), where the formation of Ca-formate complexes is weak and does not contribute significantly to the sorption on C–S–H phases. Formate shows a comparable sorption on all solids investigated.

4. Conclusions

This study provides key insights on the uptake of formate and gluconate by C–S–H, AFm phases, ettringite and hydrated cement (PC).

- The formation of formate(gluconate)-AFm phases has been investigated and characterized. A well crystalline layered structure has been observed for FOR-AFm. In agreement with the study of (Pöllman, 1989) a trigonal geometry has been assigned. The analysis of the GLU-AFm structure indicated the formation of a main AFm phase with a d-spacing = 10.3 Å due to the partial intercalation of gluconate in the interlayer region. Two further GLU-AFm phases with different water content have been also observed. The synthesis of formate or gluconate containing ettringite did not result in the formation of ettringite-like phases.
- Gluconate sorbs more strongly on AFm phases and ettringite than formate without affecting significantly the crystalline structure. The weaker uptake of formate depends mainly on the weak electrostatic interactions occurring between the positively charged surface sites of AFm and ettringite and the negatively charged formate.
- Ca plays a key role in gluconate sorption mechanism on C–S–H. Higher calcium concentration increases the gluconate sorption on C–S–H and hydrated Portland cements due the formation of Ca-gluconate surface complexes on C–S–H. An increase in sorption on C–S–H phases mediated by the formation of calcium surface complexes has also been reported for citrate (Guidone et al., 2024) and α-ISA (Pointeau et al., 2008). The chemical similarities of gluconate

and α-ISA result in a comparable and strong uptake on cement phases and PC.

- In contrast, calcium plays no significant role for the uptake of formate by C–S–H. Generally, formate sorbs relatively weak on C–S–H and hydrated PC, with R_d values in the range of 4–9 $dm^3 \cdot kg^{-1}$.
- The observed difference between formate, citrate and gluconate, as well as the similarity in the uptake of α-ISA and gluconate, illustrate the strong effect of the functional groups and their structural arrangement of the organic ligand on the sorption affinity.

CRediT authorship contribution statement

Rosa Ester Guidone: Writing – review & editing, Writing – original draft, Validation, Methodology, Investigation, Conceptualization. **Xavier Gaona:** Writing – review & editing, Validation, Supervision, Conceptualization. **Marcus Altmaier:** Writing – review & editing, Project administration, Funding acquisition. **Barbara Lothenbach:** Writing – review & editing, Validation, Supervision, Methodology, Conceptualization.

Declaration of competing interest

The authors declare the following financial interests/personal relationships which may be considered as potential competing interests: KIT - Empa reports financial support was provided by European Union. The authors declare that they have no known competing financial interests or personal relationships that could have appeared to influence the work reported in this paper.

Data availability

Data will be made available on request.

Acknowledgement

The support and expertise of Horst Geckeis (KIT) and Frank Winnefeld (Empa) is gratefully acknowledged. The EURAD-CORI project leading to this application has received funding from the European Union's Horizon 2020 research and innovation programme under grant agreement No 847593.

Appendix A. Supplementary data

Supplementary data to this article can be found online at https://doi.org/10.1016/j.apgeochem.2024.106145.

References

Aimoz, L., Wieland, E., Taviot-Guého, C., Dähn, R., Vespa, M., Churakov, S.V., 2012. Structural insight into iodide uptake by AFm phases. Environ. Sci. Technol. 46, 3874–3881.
Allmann, R., 1977. Refinement of hybrid layer structure ($Ca_2Al(OH)_6^+$ (12 SO_4 $3H_2O$). Neues Jahrbuch Mineral. Monatsh. 136–144.
Androniuk, I., Landesman, C., Henocq, P., Kalinichev, A.G., 2017. Adsorption of gluconate and uranyl on CSH phases: combination of wet chemistry experiments and molecular dynamics simulations for the binary systems. Phys. Chem. Earth, Parts A/B/C 99, 194–203.
Balonis, M., Lothenbach, B., Le Saout, G., Glasser, F.P., 2010. Impact of chloride on the mineralogy of hydrated Portland cement systems. Cement Concr. Res. 40, 1009–1022.
Balonis, M., Medala, M., Glasser, F.P., 2011. Influence of calcium nitrate and nitrite on the constitution of AFm and AFt cement hydrates. Adv. Cement Res. 23, 129–143.
Baquerizo, L.G., Matschei, T., Scrivener, K.L., Saeidpour, M., Wadsö, L., 2015. Hydration states of AFm cement phases. Cement Concr. Res. 73, 143–157.
Baur, I., Johnson, C.A., 2003. The solubility of selenate-AFt (3CaO· Al2O3· 3CaSeO4· 37.5 H2O) and selenate-AFm (3CaO· Al2O3· CaSeO4· xH2O). Cement Concr. Res. 33, 1741–1748.
Bouzouaid, L., Lothenbach, B., Fernandez-Martinez, A., Labbez, C., 2021. Portlandite solubility and Ca2+ activity in presence of gluconate and hexitols. Cement Concr. Res. 149, 106563.
Bouzouaid, L., Lothenbach, B., Fernandez-Martinez, A., Labbez, C., 2022. Gluconate and hexitols effects on CSH solubility. Cement Concr. Res. 160, 106894.
Buttler, F., Dent Glasser, L., Taylor, H., 1959. Studies on 4CaOAl2. O3. 13H2O and the related natural mineral hydrocalumite. J. Am. Ceram. Soc. 42, 121–126.
Dalconi, M.C., Artioli, G., Masciocchi, N., Giacobbe, C., Castiglioni, F., Ferrari, G., 2021. The crystal structure of a new calcium aluminate phase containing formate. Cement Concr. Res. 146, 106490.
François, M., Renaudin, G., Evrard, O., 1998. A cementitious compound with composition 3CaO. Al2O3. CaCO3. 11H2O. Acta Crystallographica Section C: Crystal Structure Communications 54, 1214–1217.
García, D., Henocq, P., Riba, O., López-García, M., Madé, B., Robinet, J.-C., 2020. Adsorption behaviour of isosaccharinic acid onto cementitious materials. Appl. Geochem. 118, 104625.
Gebler, S., 1983. Evaluation of calcium formate and sodium formate as accelerating admixtures for Portland cement concrete. Journal Proceedings 439–444.
Glaus, M.A., Laube, A., Van Loon, L.R., 2006. Solid–liquid distribution of selected concrete admixtures in hardened cement pastes. Waste Manag. 26, 741–751.
Grangeon, S., Claret, F., Linard, Y., Chiaberge, C., 2013. X-ray diffraction: a powerful tool to probe and understand the structure of nanocrystalline calcium silicate hydrates. Acta Crystallogr. B: Structural Science, Crystal Engineering and Materials 69, 465–473.
Guidone, R.E., Gaona, X., Winnefeld, F., Altmaier, M., Geckeis, H., Lothenbach, B., 2024. Citrate sorption on cement hydrates. Cement Concr. Res. 178, 107404.
Haas, J., Nonat, A., 2015. From C–S–H to C–A–S–H: experimental study and thermodynamic modelling. Cement Concr. Res. 68, 124–138.
Hartmann, A., Khakhutov, M., Buhl, J.-C., 2014. Hydrothermal synthesis of CSH-phases (tobermorite) under influence of Ca-formate. Mater. Res. Bull. 51, 389–396.
Heikal, M., 2004. Effect of calcium formate as an accelerator on the physicochemical and mechanical properties of pozzolanic cement pastes. Cement Concr. Res. 34, 1051–1056.
Helgeson, H.C., Kirkham, D.H., Flowers, G.C., 1981. Theoretical prediction of the thermodynamic behavior of aqueous electrolytes by high pressures and temperatures; IV, Calculation of activity coefficients, osmotic coefficients, and apparent molal and standard and relative partial molal properties to 600 degrees C and 5kb. Am. J. Sci. 281, 1249–1516.
Hewlet, P., 1998. Lea's Chemistry of Cement and Concrete. Arnold, London.
Jo, Y., Androniuk, I., Çevirim-Papaioannou, N., de Blochouse, B., Altmaier, M., Gaona, X., 2022. Uptake of chloride and iso-saccharinic acid by cement: sorption and molecular dynamics studies on HCP (CEM I) and CSH phases. Cement Concr. Res. 157, 106831.
Kaneko, S., Tanabe, H., Sasoh, M., Takahashi, R., Shibano, T., Tateyama, S., 2002. A Study on the Chemical Forms and Migration Behavior of Carbon-14 Leached from the Simulated Hull Waste in the Underground Condition, 757. MRS Online Proceedings Library (OPL).
Kulik, D.A., 2011. Improving the structural consistency of CSH solid solution thermodynamic models. Cement Concr. Res. 41, 477–495.
Kulik, D.A., Wagner, T., Dmytrieva, S.V., Kosakowski, G., Hingerl, F.F., Chudnenko, K.V., Berner, U.R., 2013. GEM-Selektor geochemical modeling package: revised algorithm and GEMS3K numerical kernel for coupled simulation codes. Comput. Geosci. 17, 1–24.
Kutus, B., Gaona, X., Pallagi, A., Pálinkó, I., Altmaier, M., Sipos, P., 2020. Recent advances in the aqueous chemistry of the calcium (II)-gluconate system–Equilibria, structure and composition of the complexes forming in neutral and in alkaline solutions. Coord. Chem. Rev. 417, 213337.
Kuzel, H.-J., Pöllmann, H., 1991. Hydration of C3A in the presence of Ca (OH) 2, CaSO4· 2H2O and CaCO3. Cement Concr. Res. 21, 885–895.
L'Hôpital, E., Lothenbach, B., Le Saout, G., Kulik, D., Scrivener, K., 2015. Incorporation of aluminium in calcium-silicate-hydrates. Cement Concr. Res. 75, 91–103.
Labbez, C., Pochard, I., Jönsson, B., Nonat, A., 2011. CSH/solution interface: experimental and Monte Carlo studies. Cement Concr. Res. 41, 161–168.
Leisinger, S.M., Lothenbach, B., Saout, G.L., Kägi, R., Wehrli, B., Johnson, C.A., 2010. Solid solutions between CrO4-and SO4-ettringite Ca6 (Al (OH) 6) 2 [(CrO4) x (SO4) 1-x] 3* 26 H2O. Environ. Sci. Technol. 44, 8983–8988.
Li, B., Lv, X., Dong, Y., Zhou, S., Zhang, J., 2018. Comparison of the retarding mechanisms of sodium gluconate and amino trimethylene phosphonic acid on cement hydration and the influence on cement performance. Construct. Build. Mater. 168, 958–965.
Li, G., He, T., Hu, D., Shi, C., 2012. Effects of two retarders on the fluidity of pastes plasticized with aminosulfonic acid-based superplasticizers. Construct. Build. Mater. 26, 72–78.
Lindgård, J., Andiç-Çakır, Ö., Fernandes, I., Rønning, T.F., Thomas, M.D., 2012. Alkali–silica reactions (ASR): literature review on parameters influencing laboratory performance testing. Cement Concr. Res. 42, 223–243.
Liu, X., Feng, P., Li, W., Geng, G., Huang, J., Gao, Y., Mu, S., Hong, J., 2021. Effects of pH on the nano/micro structure of calcium silicate hydrate (CSH) under sulfate attack. Cement Concr. Res. 140, 106306.
Lothenbach, B., Durdzinski, P., De Weerdt, K., 2016. Thermogravimetric Analysis. A Practical Guide to Microstructural Analysis of Cementitious Materials, 1, pp. 177–211.
Lothenbach, B., Kulik, D.A., Matschei, T., Balonis, M., Baquerizo, L., Dilnesa, B., Miron, G.D., Myers, R.J., 2019. Cemdata18: a chemical thermodynamic database for hydrated Portland cements and alkali-activated materials. Cement Concr. Res. 115, 472–506.
Lothenbach, B., Nedyalkova, L., Rojo, H., Wieland, E., Mäder, U., Tits, J., 2024. Sorption of Se(VI) and Se(IV) on AFm phases. Appl. Geochem. This issue.

Lumsden, J.S., 1902. XXXIV.—solubilities of the calcium salts of the acids of the acetic series. J. Chem. Soc. Trans. 81, 350–362.
Ma, B., Fernandez-Martinez, A., Grangeon, S., Tournassat, C., Findling, N., Claret, F., Koishi, A., Marty, N.C., Tisserand, D., Bureau, S., 2017. Evidence of multiple sorption modes in layered double hydroxides using Mo as structural probe. Environ. Sci. Technol. 51, 5531–5540.
Ma, S., Li, W., Zhang, S., Ge, D., Yu, J., Shen, X., 2015. Influence of sodium gluconate on the performance and hydration of Portland cement. Construct. Build. Mater. 91, 138–144.
Mesecke, K., Warr, L.N., Malorny, W., 2022. Structure modeling and quantitative X-ray diffraction of C-(A)-SH. J. Appl. Crystallogr. 55, 133–143.
Meyn, M., Beneke, K., Lagaly, G., 1990. Anion-exchange reactions of layered double hydroxides. Inorg. Chem. 29, 5201–5207.
Nafee, M.M., Akhtar, U.S., Islam, M.S., Halim, M.E., Mostafa, M.G., Haque, I., 2023. Synthesis and characterization of sodium gluconate and its effects on the properties of Portland cement. Int. Res. J. Pure Appl. Chem. 24, 20–32.
Nalet, C., Nonat, A., 2016. Ionic complexation and adsorption of small organic molecules on calcium silicate hydrate: relation with their retarding effect on the hydration of C3S. Cement Concr. Res. 89, 97–108.
Nedyalkova, L., Lothenbach, B., Renaudin, G., Mäder, U., Tits, J., 2019. Effect of redox conditions on the structure and solubility of sulfur-and selenium-AFm phases. Cement Concr. Res. 123, 105803.
Nedyalkova, L., Tits, J., Bernard, E., Wieland, E., Mäder, U., 2021. Sorption experiments with HTO, 36-Cl, 125-I and 14-C labeled formate on aged cement matrices retrieved from long-term in-situ rock laboratory experiments. J. Adv. Concr. Technol. 19, 811–829.
Nedyalkova, L., Tits, J., Renaudin, G., Wieland, E., Mäder, U., Lothenbach, B., 2022. Mechanisms and thermodynamic modelling of iodide sorption on AFm phases. J. Colloid Interface Sci. 608, 683–691.
Ochs, M., Mallants, D., Wang, L., 2016. Radionuclide and Metal Sorption on Cement and Concrete. Springer.
Okoronkwo, M.U., Balonis, M., Katz, L., Juenger, M., Sant, G., 2018. A thermodynamics-based approach for examining the suitability of cementitious formulations for solidifying and stabilizing coal-combustion wastes. J. Environ. Manag. 217, 278–287.
Pallagi, A., Sebők, P., Forgó, P., Jakusch, T., Pálinkó, I., Sipos, P., 2010. Multinuclear NMR and molecular modelling investigations on the structure and equilibria of complexes that form in aqueous solutions of Ca2+ and gluconate. Carbohydr. Res. 345, 1856–1864.
Perez, J.-P., 2007. The mechanism of action of sodium gluconate on the fluidity and set of Portland cement. 12th International Congress on the Chemistry of Cement.
Perkins, R.B., Palmer, C.D., 2000. Solubility of Ca6 [Al (OH) 6] 2 (CrO4) 3· 26H2O, the chromate analog of ettringite; 5–75° C. Appl. Geochem. 15, 1203–1218.
Pointeau, I., Coreau, N., Reiller, P.E., 2008. Uptake of anionic radionuclides onto degraded cement pastes and competing effect of organic ligands. Radiochim. Acta 96, 367–374.
Pöllman, H., 1989. Minelarogisch-Kristallographische Untersuchugen an Hydratationsprodukten der Aluminatphase hydraulischer Bindemittel (Teil 1). Naturwissenschaftlichen Fakultät. Friedrich-Alexander Universität, Erlagen-Nürnberg, p. 288.
Pöllmann, H., Witzke, T., Kohler, H., 1997. Kuzelite,[(SO4)· 6H2O], a New Mineral from Maroldsweisach/Bavaria. Neues Jahrbuch für Mineralogie-Monatshefte, Germany, pp. 423–432.
Runčevski, T., Dinnebier, R.E., Magdysyuk, O.V., Pöllmann, H., 2012. Crystal structures of calcium hemicarboaluminate and carbonated calcium hemicarboaluminate from synchrotron powder diffraction data. Acta Crystallographica Section B: Structural Science 68, 493–500.
Shock, E.L., 1995. Organic acids in hydrothermal solutions; standard molal thermodynamic properties of carboxylic acids and estimates of dissociation constants at high temperatures and pressures. Am. J. Sci. 295, 496–580.
Shock, E.L., Koretsky, C.M., 1995. Metal-organic complexes in geochemical processes: estimation of standard partial molal thermodynamic properties of aqueous complexes between metal cations and monovalent organic acid ligands at high pressures and temperatures. Geochem. Cosmochim. Acta 59, 1497–1532.
Shock, E.L., Sassani, D.C., Willis, M., Sverjensky, D.A., 1997. Inorganic species in geologic fluids: correlations among standard molal thermodynamic properties of aqueous ions and hydroxide complexes. Geochem. Cosmochim. Acta 61, 907–950.
Singh, N., 1976. Effect of gluconates on the hydration of cement. Cement Concr. Res. 6, 455–460.
Tasi, A., Gaona, X., Rabung, T., Fellhauer, D., Rothe, J., Dardenne, K., Lützenkirchen, J., Grivé, M., Colàs, E., Bruno, J., 2021. Plutonium retention in the isosaccharinate–cement system. Appl. Geochem. 126, 104862.
Taylor, H., 1973. Crystal structures of some double hydroxide minerals. Mineral. Mag. 39, 377–389.
Taylor, R., Richardson, I., Brydson, R., 2010. Composition and microstructure of 20-year-old ordinary Portland cement–ground granulated blast-furnace slag blends containing 0 to 100% slag. Cement Concr. Res. 40, 971–983.
Tits, J., Bradbury, M., Eckert, P., Schaible, A., Wieland, E., 2002. The Uptake of Eu (III) and Th (IV) by Calcite under Hyperalkaline Conditions: the Influence of Gluconic and Isosaccharinic Acid, PSI. Paul Scherrer Institute.
Traynor, B., Uvegi, H., Olivetti, E., Lothenbach, B., Myers, R.J., 2020. Methodology for pH measurement in high alkali cementitious systems. Cement Concr. Res. 135, 106122.
Van Loon, L.R., Glaus, M.A., 1998. Experimental and Theoretical Studies on Alkaline Degradation of Cellulose and its Impact on the Sorption of Radionuclides.
Vdovin, E., Stroganov, V., 2020. Modification of cement-bound mixtures with sodium formate additives for the construction of pavement bases at low air temperatures. In: IOP Conference Series: Materials Science and Engineering. IOP Publishing, 012065.
Vollpracht, A., Lothenbach, B., Snellings, R., Haufe, J., 2016. The pore solution of blended cements: a review. Mater. Struct. 49, 3341–3367.
von Daake, H., Stephan, D., 2017. Adsorption kinetics of retarding admixtures on cement with time controlled addition. Cement Concr. Res. 102, 119–126.
Von Hoessle, F., Plank, J., Leroux, F., 2015. Intercalation of sulfonated melamine formaldehyde polycondensates into a hydrocalumite LDH structure. J. Phys. Chem. Solid. 80, 112–117.
Wagner, T., Kulik, D.A., Hingerl, F.F., Dmytrieva, S.V., 2012. GEM-Selektor geochemical modeling package: TSolMod library and data interface for multicomponent phase models. Can. Mineral. 50, 1173–1195.
Wang, Q., Taviot-Gueho, C., Leroux, F., Ballerat-Busserolles, K., Bigot, C., Renaudin, G., 2018. Superplasticizer to layered calcium aluminate hydrate interface characterized using model organic molecules. Cement Concr. Res. 110, 52–69.
Wieland, E., 2014. Sorption data base for the cementitious near-field of L/ILW and ILW repositories for provisional safety analyses for SGT-E2. Paul Scherrer Institute (PSI).
Wieland, E., Hummel, W., 2015. Formation and stability of 14C-containing organic compounds in alkaline iron-water systems: preliminary assessment based on a literature survey and thermodynamic modelling. Mineral. Mag. 79, 1275–1286.
Wieland, E., Jakob, A., Tits, J., Lothenbach, B., Kunz, D., 2016. Sorption and diffusion studies with low molecular weight organic compounds in cementitious systems. Appl. Geochem. 67, 101–117.
Wieland, E., Lothenbach, B., Glaus, M., Thoenen, T., Schwyn, B., 2014. Influence of superplasticizers on the long-term properties of cement pastes and possible impact on radionuclide uptake in a cement-based repository for radioactive waste. Appl. Geochem. 49, 126–142.
Yan, Y., Yang, S.-Y., Miron, G.D., Collings, I.E., L'Hôpital, E., Skibsted, J., Winnefeld, F., Scrivener, K., Lothenbach, B., 2022. Effect of alkali hydroxide on calcium silicate hydrate (CSH). Cement Concr. Res. 151, 106636.
Zhang, X., He, Y., Lu, C., Huang, Z., 2017. Effects of sodium gluconate on early hydration and mortar performance of Portland cement-calcium aluminate cement-anhydrite binder. Construct. Build. Mater. 157, 1065–1073.
Zou, F., Tan, H., Guo, Y., Ma, B., He, X., Zhou, Y., 2017. Effect of sodium gluconate on dispersion of polycarboxylate superplasticizer with different grafting density in side chain. J. Ind. Eng. Chem. 55, 91–100.